The landscape of L-functions: degree 3 and conductor 1

Contemporary Mathematics
Volume **796**, 2024
https://doi.org/10.1090/conm/796/16007

The landscape of L-functions: degree 3 and conductor 1

David W. Farmer, Sally Koutsoliotas, Stefan Lemurell,
and David P. Roberts

Abstract. We extend previous lists by numerically computing approximations to many L-functions of degree $d = 3$, conductor $N = 1$, and small spectral parameters. We sketch how previous arguments extend to show that for very small spectral parameters there are no such L-functions. Using the case $(d, N) = (3, 1)$ as a guide, we explain how the set of all L-functions with any fixed invariants (d, N) can be viewed as a landscape of points in a $(d-1)$-dimensional Euclidean space. We use Plancherel measure to identify the expected density of points for large spectral parameters for general (d, N). The points from our data are close to the origin and we find that they have smaller density.

1. Introduction

1.1. Overview via pictures. Consider the set $\mathcal{L}_{d,N}$ of all automorphic L-functions of degree d and conductor N, as defined in Section 2. It decomposes as a disjoint union of its subsets of algebraic and transcendental L-functions,

$$\mathcal{L}_{d,N} = \mathcal{L}_{d,N}^{\mathrm{alg}} \sqcup \mathcal{L}_{d,N}^{\mathrm{trans}}. \tag{1.1}$$

The algebraic part is of particular interest because it conjecturally agrees with the set of analytically-normalized motivic L-functions of the given degree and conductor. But the transcendental part is of great interest too, in part because for $d \geq 3$ it is much larger than the algebraic part. Tabulation efforts, such as the LMFDB, have focused mainly on $\mathcal{L}_{d,N}^{\mathrm{alg}}$ and, via classical Maass wave forms, $\mathcal{L}_{2,N}$. In this paper, a sequel to [**6**], we aim to bring more computational attention to the very large sets $\mathcal{L}_{d,N}^{\mathrm{trans}}$ for $d \geq 3$. We focus on the first case $(d, N) = (3, 1)$.

We think about the sets $\mathcal{L}_{d,N}$ visually, with L-functions being represented by points in regions of coordinatized $(d-1)$-dimensional Euclidean spaces. Each of these ***L-points*** has a natural attached multiplicity, usually 1. A region together with its collection of L-points is a ***landscape***. We have two organizational schemes. One breaks $\mathcal{L}_{d,N}$ into $\lfloor (d+2)^2/4 \rfloor$ disjoint parts and places each part in its own ***parameter landscape***. The other places all the points in a single ***coefficient landscape***, where the region is all of $\mathbb{R}^{d-1}$. The names come from the nature of the coordinates, which are real and imaginary parts of spectral parameters in

Key words and phrases. L-function, functional equation, Maass form, spectral parameters, Plancherel measure.

A portion of this work was supported by the National Science Foundation.

the first organizational scheme, and coefficients $c_2, \ldots, c_d$ of a polynomial in the second.

For our case $(d, N) = (3, 1)$, Figure 3.1 and Figure 3.2 each draw a parameter landscape, while Figure 3.3 superimposes two similar parameter landscapes. The two remaining parameter landscapes for $(d, N) = (3, 1)$ are theoretically obstructed from having L-points, a special feature of the small conductor $N = 1$, and hence not drawn. Figure 5.2 draws the coefficient landscape, with the contribution of each parameter landscape being indicated via color. It becomes computationally more difficult to find L-functions as one goes further away from the origin in a given parameter space, and all our figures are of course partial in that they only show the known L-points. Also our methods are numerical, so some L-points could conceivably be incorrect, although we think this is unlikely. We encourage the reader to turn to these four figures, because they give an accurate first sense of the content of this paper.

We are interested in understanding the landscapes both computationally, as just indicated, and theoretically. The foundational theoretical concepts are ***Plancherel measure*** μ_d and its ***canonical approximation*** μ'_d. Attention to these concepts is a significant advance in this paper beyond the results of [**6**]. The very similar measures μ_d and μ'_d are indicated by contour plots on our three figures of parameter landscapes. They are not indicated directly on the coefficient landscape because they do not need to be: $\mu'_d = P_d\, dc_2 \cdots dc_d$ is exactly Euclidean. The meaning of μ_d is that it conjecturally governs the distribution of L-points in a precise asymptotic sense. We combine three formulas from the literature to identify the ***Plancherel constants*** P_d. The relevant one for our case is

$$P_3 = \frac{\sqrt{3}\zeta(3)}{128\pi^3} \approx 0.0005246. \tag{1.2}$$

While our new data is only in the $(d, N) = (3, 1)$ case, our text works with general (d, N) as it is aimed at supporting future numerical investigations.

1.2. Content of the sections. Section 2 defines the sets $\mathcal{L}_{d,N}$, reviews standard material about L-functions, and defines the $\lfloor (d+2)^2/4 \rfloor$ receiver regions for the parameter landscapes. Section 3 populates the landscapes with L-points, following the methods of [**6**]. Section 4 offers reminders that each individual L-function is interesting and sketches how one can prove that parameter landscapes with sufficiently small conductor N have an L-point-free region near their origin.

Section 5 discusses the purely algebraic passage from parameter landscapes to the coefficient landscape by means of symmetric functions. Section 6 gives the Plancherel theory including the identification of the constants P_d. Our data gives points at roughly half the asymptotic density P_d. We explain by comparison with the well-understood $d = 2$ case that this is an expected shortfall; there should be as yet undiscovered secondary terms which will make theory better match the data. Finally Section 7 gives two independent complements. One compares our data with the p-adic Plancherel measures on the class space of SU_3, finding again the need for secondary terms. The other discusses the extent to which transcendental L-functions outnumber algebraic L-functions in degrees ≥ 3.

1.3. Availability of data. The L-functions in $\mathcal{L}_{3,1}$ have the form

$$L(s) = \prod_{\text{primes } p} \frac{1}{1 - a_p p^{-s} + \overline{a}_p p^{-2s} - p^{-3s}}. \tag{1.3}$$

For each drawn L-point, its coordinates in the landscape and the complex numbers a_p to their computed precision are available on GitHub at [**8**], and code to compute the L-points is at [**15**]. Earlier data, dating back to [**3**, **4**, **6**], is already conveniently available on the LMFDB for $(d, N) \in \{(3,1), (3,4), (3,9), (4,1)\}$. We plan to systematically extend this section of the LMFDB, because much more is within computational reach.

2. Background on L-functions

Here we review L-functions with an initial focus on the fundamental decomposition of all automorphic L-functions into the two types,

$$\mathcal{L} = \mathcal{L}^{\text{alg}} \sqcup \mathcal{L}^{\text{trans}}. \tag{2.1}$$

Whether an automorphic L-function is algebraic or transcendental depends only on the Γ-factor in its functional equation and our second main focus is the space X_d of possible Γ-factors in degree d, and various related spaces.

2.1. The set of automorphic L-functions $\mathcal{L}$. As a terminological catch-all, define an ***L-function*** to be a Dirichlet series with Euler product converging in some right half plane:

$$L(s) = \prod_{\text{primes } p} \frac{1}{f_p(p^{-s})} = \sum_{n=1}^{\infty} \frac{a_n}{n^s}; \tag{2.2}$$

here the $f_p(x) = 1 + \cdots$ are required to be polynomials in $\mathbb{C}[x]$ having a maximal ***degree*** d. For example, the Riemann zeta function $\zeta(s)$ has $f_p(x) = 1 - x$ for all p and degree 1. The class of L-functions just defined is very large. Its purpose is to give a uniform language for talking about some of its subsets, namely automorphic, motivic, and our experimental L-functions.

An ***automorphic L-function*** for this paper is an L-function associated in the standard way to a balanced tempered-at-∞ cuspidal automorphic representation of the adelic group $GL_d(\mathbb{A})$. We do not need to enter into the very complicated automorphic theory, as we will just be using known properties of these L-functions. A list of known properties which moreover conjecturally characterizes automorphic L-functions is given in [**9**]. Here we review what we need.

Associated to an automorphic L-function is a ***conductor*** $N \in \mathbb{Z}_{\geq 1}$. Also associated is a ***central character*** χ, which is a Dirichlet character mod N. So $\chi : \mathbb{Z}/N \to \mathbb{C}$ is multiplicative, and $\chi(p) = 0$ for the primes p dividing N. The L-functions coming from $GL_d(\mathbb{A})$ have degree d, as

$$f_p(x) = 1 - a_p x + \cdots + (-1)^d \chi(p) x^d.$$

The Riemann zeta function is automorphic, and has a meromorphic continuation to the whole plane with a unique pole at $s = 1$. All other automorphic L-functions are entire. The completed L-function and its functional equation take the form

$$\Lambda(s) := L(s)\, N^{s/2} \prod_{j=1}^{d_1} \Gamma_{\mathbb{R}}(s + \mu_j) \prod_{k=1}^{d_2} \Gamma_{\mathbb{C}}(s + \nu_k) = \varepsilon \overline{\Lambda}(1 - s). \tag{2.3}$$

Here the bar indicates Schwarz reflection, so that $\overline{L}(s) = \overline{L(\overline{s})} = \sum_n \overline{a}_n n^{-s}$ is the ***dual*** of L. Also $\Gamma_{\mathbb{R}}$ and $\Gamma_{\mathbb{C}}$ are the normalized Γ-functions,

$$\Gamma_{\mathbb{R}}(s) = \pi^{-s/2}\Gamma(s/2), \qquad \Gamma_{\mathbb{C}}(s) = 2(2\pi)^{-s}\Gamma(s). \tag{2.4}$$

The double product of Γ-functions in (2.3) is the Γ-***factor*** of L, to be discussed in more detail in the next subsection. The ***sign*** ε is a complex number on the unit circle. The $d_i \in \mathbb{Z}_{\geq 0}$ satisfy $d_1 + 2d_2 = d$ and form the **signature** (d_1, d_2) of L.

2.2. Γ-factors. Much of this paper is driven by the nature of Γ-factors, and so the terms introduced in this section are particularly important. The ***spectral parameters*** μ_j and ν_k in (2.3) are written in terms of their real and imaginary parts as

$$\mu_j = \delta_j + i\lambda_j, \qquad \nu_k = \kappa_k + i\beta_k.$$

They are constrained by the ***balanced*** condition in our definition of automorphic L-function, $\sum \lambda_j + 2\sum \beta_k = 0$. They are constrained also by the ***tempered-at-∞*** condition, which requires $\delta_j \in \{0, 1\}$ and $\kappa_k \in \{\frac{1}{2}, 1, \frac{3}{2}, 2, \dots\}$. There is no ambiguity in d_1 and d_2 coming from the duplication formula $\Gamma_{\mathbb{C}}(s) = \Gamma_{\mathbb{R}}(s)\Gamma_{\mathbb{R}}(s+1)$ because $\kappa_k = 0$ is disallowed. Important for us is the ***refined signature*** (d_+, d_-, d_2), where d_+ and d_- are the number of j with $\delta_j = 0$ and $\delta_j = 1$ respectively. Henceforth, we write λ_{d_1+k} rather than β_k. To remove ambiguities, we require that both the μ_j and the ν_k are non-decreasing with respect to the standard lexicographical order on $\mathbb{C}$.

The Γ-***type*** of a Γ-factor is the list of δ_j followed by the list of $2\kappa_k$. For example, a degree seven L-function might have Γ-type $(0, 0, 1, 1, 1; 5)$. Following LMFDB conventions, we normally write Γ-types by prefixing each δ_i with an r and each $2\kappa_k$ with a c, as in $r0r0r1r1r1c5$. A Γ-type is called ***even*** if all $2\kappa_k$ are even. It is called ***odd*** if $d_1 = 0$ and all $2\kappa_k$ are odd. Thus our example Γ-type is neither odd nor even.

There is an important constraint on the spectral parameters in terms of the central character:

$$\chi(-1) = (-1)^{\sum \delta_j + \sum (2\kappa_k + 1)}. \tag{2.5}$$

Always $\chi(-1) = \epsilon_\infty^2$, where $\epsilon_\infty \in \{1, i, -1, -i\}$ depends multiplicatively on the individual Gamma factors in (2.3), in the way presented in Table 2.1. There are two simplifications when $N = 1$. First, $\chi(-1) = 1$, allowing one to disregard half the possible spectral parameters, namely those that fail (2.5). Second $\varepsilon = \epsilon_\infty$; this replaces an unknown quantity with a known one in the searches described in §3.5.

2.3. The decomposition $\mathcal{L} = \mathcal{L}^{\mathrm{alg}} \sqcup \mathcal{L}^{\mathrm{trans}}$. By definition, an automorphic L-function is ***algebraic*** if its spectral parameters are real and its Γ-type has a parity. The remaining automorphic L-functions are ***transcendental***. The next two paragraphs explain how this innocuous-looking decomposition is expected to be a very sharp dichotomy.

We do not need to be precise about ***motivic L-functions***. The procedure for computing them starts from counting points on a fixed algebraic variety over varying finite fields. Any motivic L-function has an associated Γ-factor coming from Hodge theory. We assume a primitivity condition corresponding to focusing attention on an irreducible motive. After switching to the analytic normalization, a change of variables of the form $s \to s + \frac{w}{2}$ for w an integer, the fundamental

and widely-believed Langlands reciprocity conjecture says that motivic L-functions are automorphic. By the nature of their Γ-factors, they would have to be in $\mathcal{L}^{\mathrm{alg}}$. A conjectural converse says that all L-functions in $\mathcal{L}^{\mathrm{alg}}$ come from motives in this way.

For a motivic L-function, even in its analytic normalization, all the coefficients a_n are algebraic numbers. In contrast, for a transcendental L-function one expects that all the nonzero λ_j and almost all the nonzero a_p are transcendental numbers. Assuming that all algebraic L-functions are motivic, this conjecture translates to a contrast between the summands $\mathcal{L}^{\mathrm{alg}}$ and $\mathcal{L}^{\mathrm{trans}}$ that explains their names.

We refer the reader again to [**9**] for more details on everything discussed so far. One subtlety worth highlighting concerns Axioms 4a and 4b on the list of axioms in Section 2.1 of [**9**]. We are imposing Axiom 4a by our "temperedness-at-∞" condition, because it is necessary for our points-in-landscapes presentation. The Selberg conjecture says that we would not enlarge our set $\mathcal{L}$ if we removed this condition. We are not imposing Axiom 4b, which corresponds to a "temperedness at all finite primes p" condition, because it is not necessary for our presentation. Here the Ramanujan conjecture says that we would not decrease our set $\mathcal{L}$ if we added this condition.

2.4. The constructional problem. Consider now the problem of explicitly writing down automorphic L-functions, say in an approximate form $\sum_{n=1}^{c} a_n n^{-s}$. Assuming Langlands reciprocity, one can do this relatively easily for many algebraic L-functions by motivic methods. For example, writing down any genus g curve over $\mathbb{Q}$ and computing many a_n for it gives L-functions with Γ-factor $\Gamma_{\mathbb{C}}(s+1/2)^g$ and trivial character. However one can construct L-functions by purely automorphic methods with similar ease only for the limited class of Γ-factors appropriately related to discrete series, and even then the cutoff c typically needs to be taken much smaller. In the above example, automorphic methods are feasible in the case $g = 1$ and small conductor N, as indeed one has complete tables of newforms of weight 2 and $\Gamma_0(N)$. However constructing analogous tables for $g \geq 2$ using Siegel modular forms would be much harder.

In the case of transcendental L-functions, motivic methods are by definition not available and automorphic methods would be very difficult since Γ-factors are very far from coming from discrete series. In this paper, we do what seems like the best that can be currently done: we produce ***experimental L-functions*** $\prod_p f_p(x)^{-s}$ having only finitely many non-trivial factors, following the method reviewed in §3.5. Their purpose is to approximate actual automorphic L-functions. At present, like in typical instances of using motivic L-functions as in the last paragraph, the evidence for the existence of a corresponding automorphic L-function is strong, but not conclusive.

Having carefully made distinctions, we will now generally be more brief with our language: "L-function" in theoretical contexts will mean automorphic L-function; "L-function" in the context of our searches will mean experimental L-function. One would like to populate our landscapes with actual automorphic L-points, but we are of course populating them with experimental L-points.

2.5. Spaces of generalized Γ-factors. The material of this subsection is completely elementary. However it is not standard, but rather is particular to our concerns in this paper. To define the Euclidean regions receiving L-points, it is

necessary to allow ***generalized* Γ*-factors*** by relaxing the half-integrality condition on the κ_k to $\kappa_k \in (0,\infty)$. Let X'_{d_-,d_+,d_2} be the set of Γ-factors with refined signature (d_-,d_+,d_2). Because of our ordering convention, the λ_j and κ_k are well-defined real-valued functions on X'_{d_-,d_+,d_2}. Because of the balanced condition, the functions $(\lambda_1,\dots,\lambda_{d_1+d_2-1},\kappa_1,\dots,\kappa_{d_2})$ render X'_{d_-,d_+,d_2} a full-dimensional cone in $\mathbb{R}^{d-1}$ and thus a connected topological space. Let X'_{d_1,d_2} be the disjoint union of the $X'_{d+,d-,d_2}$ with $d_1 = d_+ + d_-$. Let X'_d likewise be the disjoint union of the X'_{d_1,d_2} with $d = d_1 + 2d_2$. So clearly X'_{d_1,d_2} has d_1+1 connected components. As reported in the introduction, the number of connected components of X'_d works out to the "quarter square" $\lfloor (d+2)^2/4 \rfloor$. As an alternative notation for X'_{d_+,d_-,d_2} we use repetition, as in $X'_{2,3,1} = X'_{++---c}$. The possible spaces X'_{d_+,d_-,d_2} with $d \le 3$ are listed in this alternative notation in Table 2.1.

TABLE 2.1. Γ-types γ and refined signatures $\delta = (d_+,d_-,d_2)$ indexing inclusions $X_\gamma \subseteq X'_\delta$ of connected spaces in degree $d \le 3$

d	$\chi(-1)$	ϵ_∞	γ	δ	Automorphic Source	γ	$\dim X'_\delta$
1	1	1	$r0$	$+$	Even Dirichlet characters	0	0
	-1	i	$r1$	$-$	Odd Dirichlet characters	0	0
2	1	1	$r0r0$	$++$	Even weight 0 Maass forms	1	1
	-1	i	$r0r1$	$+-$	Weight 1 forms	1	1
	1	-1	$r1r1$	$--$	Odd weight 0 Maass forms	1	1
	$(-1)^k$	i^k	$c2\kappa$	c	Weight $k = 2\kappa+1$ forms	0	1
3	1	1	$r0r0r0$	$+++$	Spherical Maass forms	2	2
	-1	i	$r0r0r1$	$++-$		2	2
	1	-1	$r0r1r1$	$+--$		2	2
	-1	$-i$	$r1r1r1$	$---$		2	2
	$(-1)^k$	i^k	$r0c2\kappa$	$+c$		1	2
	$(-1)^{k+1}$	i^{k+1}	$r1c2\kappa$	$-c$		1	2

The subspaces of all the above spaces consisting of possible Γ-factors are denoted by removing the prime. The connected components of X_d are indexed by their Γ-types, as discussed above. All the components of X_{d_1,d_2} have dimension d_1+d_2-1, there being infinitely many components exactly when $d_2 > 0$, indexed by κ. One of the virtues of LMFDB notation for Γ-types is that it lets one easily distinguish the connected spaces X'_{d_+,d_-,d_0} from the connected components of their subspaces X_{d_+,d_-,d_2}. As an example, $r0r0r1r1r1c5 \subset X'_{++---c}$ is an inclusion of a connected five-dimensional space into a connected six-dimensional space. In general, the notational transition is made by $r0 \to +$, $r1 \to -$, and replacing all the $2\kappa_k$'s by c's. All possibilities for $d \le 3$ are listed in Table 2.1.

2.6. Sources. While we do not need the full automorphic theory, we will reference automorphic forms in classical contexts. Very simply, it is known that $\mathcal{L}_{1,N} = \mathcal{L}^{\mathrm{alg}}_{1,N}$ is the set of Dirichlet L-functions of conductor N. In the next dimension, $\mathcal{L}_{2,N}$ is conjecturally the set $L(f,s)$ of L-functions coming from newforms on $\Gamma_1(N)$. Holomorphic forms and Maass forms with Laplacian eigenvalue $\frac{1}{4}$ give L-functions in $\mathcal{L}^{\mathrm{alg}}_{2,N}$. Maass forms with Laplacian eigenvalue $\lambda > \frac{1}{4}$ give L-functions in $\mathcal{L}^{\mathrm{trans}}_{2,N}$. There are not expected to be Maass forms with Laplacian eigenvalue $< \frac{1}{4}$

because their L-functions would be counterexamples to the Selberg conjecture; if such L-functions exist, they would not be in our $\mathcal{L}_{2,N}$. For $d \geq 3$, one is already out of the classical setting. Table 2.1 summarizes the situation.

3. The parameter landscapes for L-functions with $(d, N) = (3, 1)$

Here we draw the three pictures promised in the introduction and discuss how we found the L-functions corresponding to the L-points in the pictures.

3.1. The landscape of L-functions with Γ-type $r0r0r0$ in the cone X_{+++}. This is the landscape studied in [**6**] and we roughly double the number of L-points previously available in it. As explained in §2.5, the L-functions considered here have Γ-factor of the form

$$\Gamma_{\mathbb{R}}(s + i\lambda_1)\Gamma_{\mathbb{R}}(s + i\lambda_2)\Gamma_{\mathbb{R}}(s + i\lambda_3), \tag{3.1}$$

with $\lambda_j \in \mathbb{R}$ and $\lambda_1 + \lambda_2 + \lambda_3 = 0$. The general prescription of §2.2, useful for uniform theoretical discussions, is in this case to require $\lambda_1 \leq \lambda_2 \leq \lambda_3$, and use λ_1 and λ_2 as coordinates. Instead, we will be consistent with [**6**] and order by $\lambda_3 \leq \lambda_2 \leq \lambda_1$, still using λ_1 and λ_2. This difference in conventions is unimportant: it is a question of choosing a fundamental domain for a Euclidean plane with an action by the symmetric group S_3.

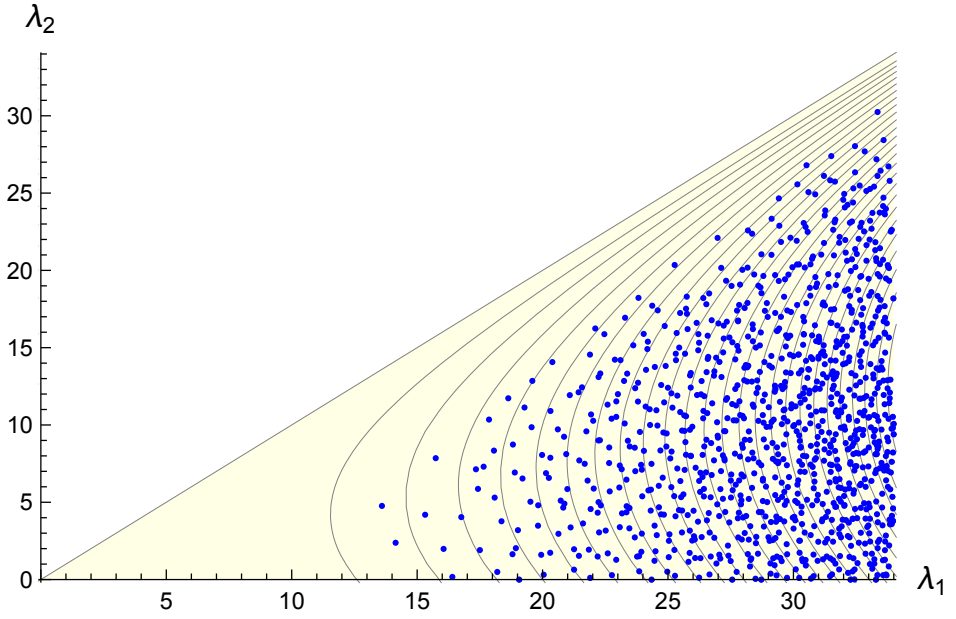

FIGURE 3.1. The L-points (λ_1, λ_2) for L-functions with Γ-type $r0r0r0$, having Γ-factor (3.1) and conductor 1.

There is a second redundancy not emphasized in the previous section: an L-function and its dual determine each other by complex conjugation. To remove this redundancy, again following [**6**], we require $\lambda_2 \geq 0$. Accordingly, Figure 3.1 draws only half of the landscape; the other half is a wedge-shaped region below the λ_1-axis, obtained by the transformation $(\lambda_1, \lambda_2) \mapsto (\lambda_1 + \lambda_2, -\lambda_2)$. So the shaded

region is a fundamental domain for the action of a dihedral group $D_6 \cong S_3 \times S_2$. If we chose coordinates on the plane so that this action were isometric, the shaded region would be one-twelfth of the plane, namely a cone with base angle 30°.

There are six L-points in Figure 3.1 on the λ_1-axis. They arise as the symmetric squares of L-functions of the classical Maass forms corresponding to the six rightmost colored L-points in the left half of Figure 6.2. The coordinates $(\lambda_1, 0)$ in Figure 3.1 and (λ) in Figure 6.2 are related by $\lambda_1 = 2\lambda$. It is known that the non-algebraic self-dual L-functions in $\mathcal{L}_{1,3}$ arise in this way.

A careful look at Figure 3.1 reveals striations running approximately along lines of slope -1, 0, and 1. We will explain some aspects of these patterns in a future paper.

3.2. The landscape of L-functions with Γ-type $r0r1r1$ in the cone X_{+--}. Our second landscape is populated with L-functions with Γ-factor of the form

$$\Gamma_{\mathbb{R}}(s + i\lambda_1)\Gamma_{\mathbb{R}}(s + 1 + i\lambda_2)\Gamma_{\mathbb{R}}(s + 1 + i\lambda_3). \tag{3.2}$$

Here λ_2 and $\lambda_3 = -\lambda_1 - \lambda_2$ are playing the same role and so we normalize by requiring $\lambda_2 \geq \lambda_3$. The bottom boundary of the drawn region comes from the equation $\lambda_2 = \lambda_3$, i.e. $2\lambda_1 + \lambda_2 = 0$. As λ_1 is playing a different role from the other two λ_i, we can remove the redundancy of duality by restricting attention to $\lambda_1 \geq 0$. So the highlighted region is a fundamental domain for a group of the form $C_2 \times C_2$, and so really should be thought of as one-quarter of the full plane.

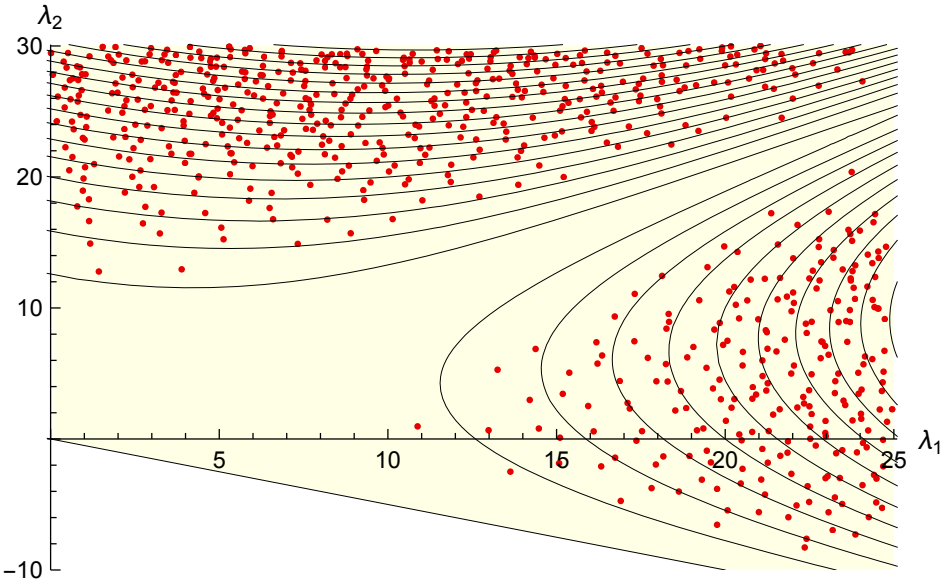

FIGURE 3.2. The L-points (λ_1, λ_2) for L-functions with Γ-type $r0r1r1$ having Γ-factor (3.2) and conductor 1.

In contrast with the previous subsection, where all L-functions have sign 1, here all L-functions have sign -1, by Table 2.1. These signs are important in our search for L-functions. However, the sign being -1 does not force central vanishing of the

L-functions, since they are not self-dual. Applying general principles to our cases here, we would expect that $L(1/2) \neq 0$ for all L in any $\mathcal{L}_{3,N}^{\text{trans}}$.

3.3. The landscape of $r0c2\kappa$ lines in X'_{+c} and the landscape of $r1c2\kappa$ lines in X'_{-c}. Our third case illustrates typical behavior for arbitrary d better than the first two cases. Here the L-functions have Γ-factors of the form

$$\Gamma_{\mathbb{R}}(s+\delta+i\lambda)\Gamma_{\mathbb{C}}(s+\kappa-i\lambda/2). \tag{3.3}$$

We work in the (κ,λ) plane. For $\tau \in \{+,-\}$, the set $X'_{\tau c}$ is identified with the half-space where $\kappa > 0$. Following the general prescription, a point in X'_{+c} is a generalized Γ-factor (3.3) with $\delta = 0$; similarly, points in X'_{-c} index generalized Γ-factors (3.3) with $\delta = 1$. To remove the redundancy given by duality, we draw only the quadrant where also $\lambda \geq 0$.

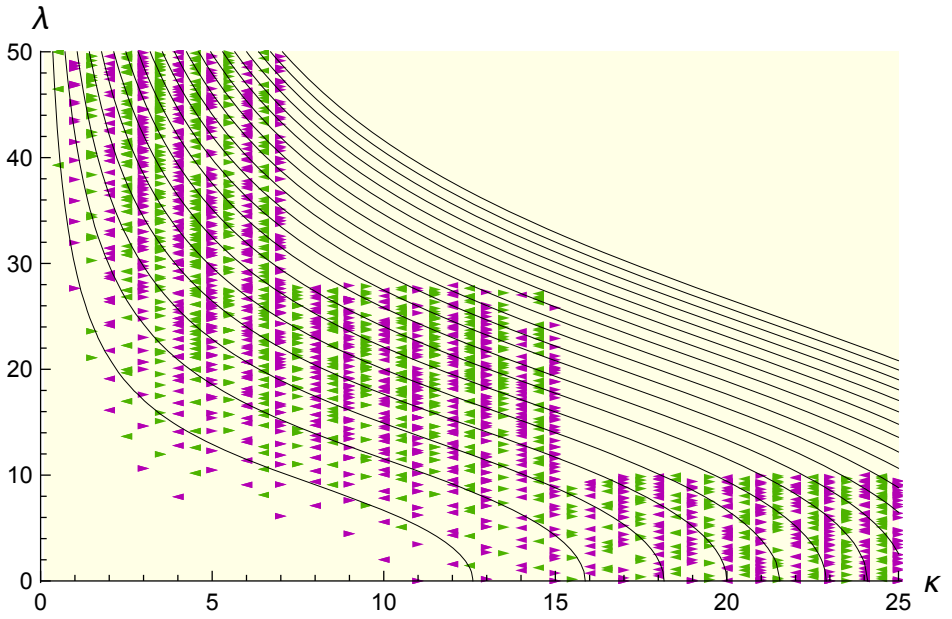

FIGURE 3.3. The L-points (κ,λ) for L-functions with Γ-type $r\delta c2\kappa$, having Γ-factor (3.3) and conductor 1. The lighter green triangles correspond to $\delta = 0$ and the darker purple triangles have $\delta = 1$. The triangles are pointing left if the sign of the functional equation is -1, and pointing right if the sign is $+1$. The blank region at the upper right has not yet been searched.

The spaces $X_{\tau c}$ of actual Γ-factors come from imposing the condition that $\kappa \in \frac{1}{2}\mathbb{Z}_{\geq 1}$. Because of the central character condition (2.5) and the identification of $\chi(-1)$ on Table 2.1, L-points in X_{-c} can only have integral κ coordinates while L-points in X_{+c} can only have half-integral κ. It is appropriate to superimpose the two landscapes in one figure, because the formula (6.3) for Plancherel measure μ on $X_{\tau 0}$ and the formula (6.4) for approximate Plancherel measure μ' on $X'_{\tau 0}$ are independent of $\tau \in \{-,+\}$. This agreement of measures holds always between the spaces indexed by (a,b,d_2) and (b,a,d_2). Thus X_{+++} from §3.1 would be naturally

superimposed with X_{---}, and X_{+--} from §3.2 would be naturally superimposed with X_{-++}. To repeat a point from the introduction, it is only because $N = 1$ that each of the latter spaces do not have L-points.

3.4. Algebraic L-points. The parts of our three landscapes which could contain algebraic L-points are just the cone tips $(0, 0)$ in Figures 3.1 and 3.2, and the points $(\kappa, 0)$ for κ a positive integer in Figure 3.3. The cone tips are in a large L-point-free region to be discussed in §4.3. So the first two figures are very far from containing algebraic L-points. This third figure does contain algebraic L-points, all coming from classical modular forms at level one via symmetric squares, in direct analogy with the construction described in §3.1. Here a holomorphic form of weight k gives an L-point at $(k - 1, 0)$. The contributing newforms have weights $k = 12$, 16, 18, 20, 22, 24, 26, and 26, and the L-point at $(25, 0)$ in Figure 3.3 is the only one in our three figures with multiplicity larger than one. The very low L-point on the $\kappa = 13$ line has $\lambda \approx 0.1660$ and is an interesting near miss. The fact that the corresponding L-function is not self-dual is seen clearly also in its first coefficients: $a_2 \approx 0.0256 - 0.7997i$ and $a_3 \approx -0.5418 + 1.2019i$ are far from real.

One has to increase conductors very significantly for algebraic L-points of various types to even exist. In the settings of Figures 3.1 and 3.2, all algebraic L-points are expected to come from representations of $\mathrm{Gal}(\overline{\mathbb{Q}}/\mathbb{Q})$ into $\mathrm{GL}_3(\mathbb{C})$ with finite image. The trace of complex conjugation is ± 3 for Figure 3.1 and ± 1 for Figure 3.2. The LMFDB tabulates all such representations of sufficiently small conductor. The smallest conductors for traces 3, -3, 1, and -1 are respectively 1957, 2828, 283, and 229. The images are respectively the groups S_4, $S_4 \times S_2$, S_4, and S_4. The L-functions are all self-dual and come from Dirichlet twists of symmetric squares of degree two L-functions. To get non-self-dual L-functions which do not come in this way from degree two L-functions, one needs even larger conductor. The case of non-self-dual algebraic L-functions in the setting of Figure 3.3 is discussed in §7.3.

3.5. The search method. Our method for locating L-points in landscapes was explained in [**6**]. We are working with more general Γ-factors, but the basic method has not changed. We give a quick summary here.

The main idea is to construct continuous functions which vanish at the L-points. We build such functions using the fact that an L-function can be evaluated in multiple ways. Given such functions, we can use the secant method to explore a landscape and locate points of simultaneous vanishing.

In more detail, the needed continuous functions are constructed using the "approximate functional equation"

$$\Lambda(s)g(s) = Q^s \sum_{n=1}^{\infty} \frac{a_n}{n^s} f_1(s, n) + \varepsilon Q^{1-s} \sum_{n=1}^{\infty} \frac{\overline{a}_n}{n^{1-s}} f_2(1 - s, n). \tag{3.4}$$

Here $Q = \sqrt{N}$ and f_1 and f_2 are integrals involving a test function $g(s)$ and the Γ-factors. By evaluating an L-function using different test functions g but at the same point s, one obtains an equation in the Dirichlet coefficients a_n. Besides these linear equations coming from (3.4) there are also non-linear equations coming from the Euler product (1.3), reducing the set of unknowns to the prime-indexed coefficients a_p.

To illustrate the idea, we sketch how we found the L-point with coordinates $(\kappa, \lambda) = (\frac{5}{2}, 16.97618\ldots)$ on Figure 3.3. We work with an associated real-valued

Z-function $Z(t)$ directly related to $L(s)$ via $s = \frac{1}{2} + it$ as discussed in §4.1 below. Consider a hypothetical (but actually non-existent) L-point with exact spectral parameters say $(\kappa, \lambda) = (\frac{5}{2}, 16.97)$. Equation (3.4) with $g(s) = 1$ and $t = 5$ says

$$Z(5) = 2.44 - 1.91a_2^r - 16.65a_2^i - 1.01a_3^r - 1.27a_3^i - 0.091a_4^r - 0.090a_4^i + \cdots \\ - 0.000023a_7^r - 0.000023a_7^i + \cdots - 5.0 \times 10^{-10}a_{11}^r - 6.2 \times 10^{-10}a_{11}^i + \cdots .$$

With $g(s) = e^{is/2}$ and $t = 5$, the equation (3.4) says

$$Z(5) = -0.145 + 0.42a_2^r - 1.54a_2^i + 0.35a_3^r + 0.29a_3^i - 0.042a_4^r + 0.032a_4^i + \cdots \\ + 0.000022a_7^r + 0.000012a_7^i + \cdots + 3.5 \times 10^{-10}a_{11}^r - 1.1 \times 10^{-0}a_{11}^i + \cdots .$$

The notation a_n^r and a_n^i refers to the real and imaginary parts of the Dirichlet coefficient a_n, respectively. The coefficients come from the integrals f_1 and f_2 and can easily be obtained to hundreds of digits of precision.

The equality of the two expressions for $Z(5)$ gives one equation in the Dirichlet coefficients. Choosing other test functions likewise gives other equations. The rapid decrease in the contributions of the coefficients enables one to truncate the expression to obtain an equation in finitely many variables. We can create more equations than unknowns and then solve a sub-system with equal number of equations and unknowns. Typically that system has a solution, and often it has several. Plugging these solutions into the unused equations (which we call "detectors") gives functions, all of which should vanish at a genuine L-point.

We repeat the process for another hypothetical (but also non-existent) L-point, say with $(\kappa, \lambda) = (\frac{5}{2}, 16.98)$. By comparing the residuals from the detectors at the two hypothetical L-points, we can use the secant method to determine a more accurate estimate for the coordinates of an actual L-point. When it is successful, our values for λ and the a_p are improved, typically by one or two additional decimal places of accuracy on each iteration. We generally stop when we are confident that we have computed the spectral parameters to at least a dozen digits of accuracy. In this example, we stopped at

$$\begin{aligned} \lambda &\approx \quad 16.9761877662491, \\ a_2 &\approx -0.063424433675 \quad + 0.10988282023\,i, \\ a_3 &\approx \quad 0.63801509281 \quad + 0.50484439411\,i, \\ a_5 &\approx \quad 0.9093205878 \quad - 0.1141574688\,i, \\ a_7 &\approx \quad 0.68168545 \quad + 0.02028876\,i, \\ a_{11} &\approx -0.33243 \quad + 0.12179\,i, \\ a_{13} &\approx -0.46 \quad - 0.72\,i. \end{aligned} \tag{3.5}$$

The same computations enable us to evaluate the L-function accurately, in this case finding $Z(5) \approx -0.03656426734$. This Z-function is the bottom one graphed in Figure 4.1.

An important point is that the test functions need to be chosen sufficiently different from each other to make the system well-conditioned. This is difficult to do when the spectral parameters are large and is a limitation of the method. Another interesting point is that we are forced to work to high precision, typically to more than 50 decimal places of accuracy, because the system is ill-conditioned and many digits of precision are lost in the calculations. Again for more details, see [**6**].

3.6. Rigor and completeness. While our methods never actually establish the existence of L-functions, it is worth emphasizing that they are capable of producing rigorous statements. For example, they can prove that there are no L-functions with spectral parameters within certain regions. Similarly, suppose one knew somehow from some external reason that a given region contains exactly one L-point. Then our methods can rigorously identify small intervals guaranteed to contain the correct coordinates of the L-point and the correct real and imaginary parts of some initial coefficients a_p.

In practice, the step in our search process where we are most likely to miss actual L-functions is in the initial scan of a region to find likely candidates. It can happen for example that search parameters which seem to work well in one region miss L-functions in a nearby region. As one leaves the origin and crosses contour lines in any of Figures 3.1, 3.2, and 3.3, we expect the percentage of L-functions that our program has found generally decreases. We expect that we have found almost all L-points up through the first few contours, but it is surely a much smaller percentage towards the end.

4. Zero-free and L-point-free regions

Each transcendental L-function should be viewed as just as remarkable an analytic object as an algebraic L-function, even though it is much harder to access computationally. We begin by considering zero-free intervals on the critical line of a given L-function and conclude by considering L-point-free regions in landscapes of L-functions. We sketch how these two topics are parallel in nature, as the explicit formula can be used to establish such regions of each type.

4.1. Three L-functions and their low-lying zeros. Every L-function has an associated Z-function, characterized up to sign by $|L(\frac{1}{2}+it)| = |Z(t)|$, with $Z(t)$ real and smooth for $t \in \mathbb{R}$. To fix the sign, we follow the LMFDB's convention of requiring that $Z(t)$ be positive for t a sufficiently small positive number. Figure 4.1 graphs the Z-function behind an L-point on each of the three figures from the previous section.

The Riemann Hypothesis for an L-function is equivalent to the assertion that the nontrivial zeros of the corresponding Z-function are real. The plots in Figure 4.1 make it appear that the Riemann Hypothesis is not true for these three L-functions. Specifically, a positive local minimum or a negative local maximum is caused by non-real zeros of the Z-function, or, equivalently, zeros off the critical line for the L-function. But the local extrema in Figure 4.1 do not point to counterexamples, because the Riemann Hypothesis is a statement about the *nontrivial* zeros of the L-function. The trivial zeros occur at the poles of the Γ-factors, and it is these trivial zeros which are causing the behavior which seems surprising at first glance. This phenomenon is difficult to see for algebraic L-functions where all the trivial zeros occur on the negative real axis.

Figure 4.2 shows how the trivial zeros appear to "push aside" the nearby zeros on the critical line. The L-functions have been chosen to all have trivial zeros at height approximately 17 to facilitate comparison. The trivial zeros at this height come from a gamma factor $\Gamma_{\mathbb{R}}(s+\delta+i\lambda)$ with $\lambda \approx -17$. The pushing is stronger in the first and third cases because the trivial zeros are one step closer: $\delta = 0$ in these cases, while $\delta = 1$ in the second case.

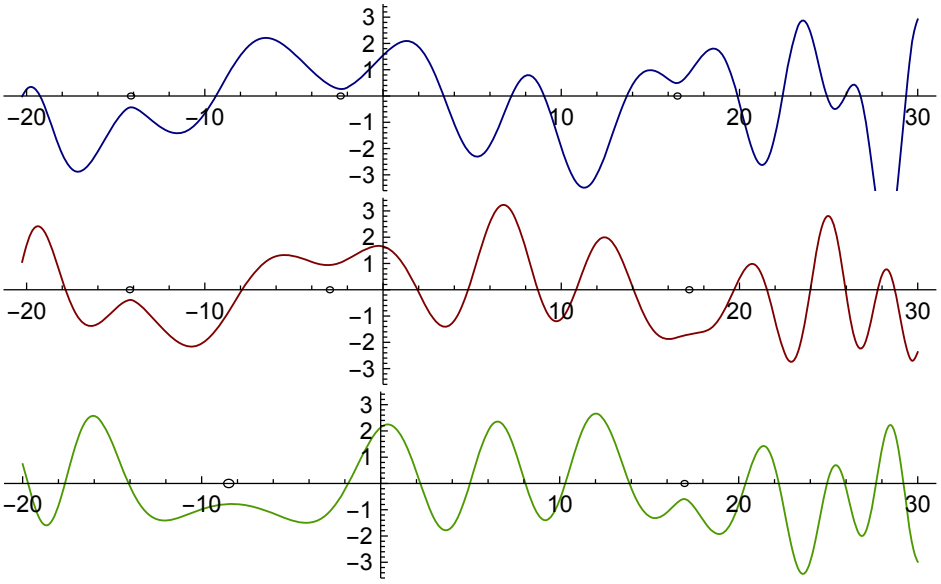

FIGURE 4.1. Three Z-functions, coming from L-functions with the following Γ-types and L-point coordinates, from top to bottom: $r0r0r0$, $(\lambda_1, \lambda_2) \approx (14.141, 2.380)$; $r0r1r1$, $(\lambda_1, \lambda_2) \approx (14.204, 2.980)$; and $r0c5$, $(\kappa, \lambda) = (\frac{5}{2}, 16.976\ldots)$. The small circles are the projections of the trivial zeros onto the critical line.

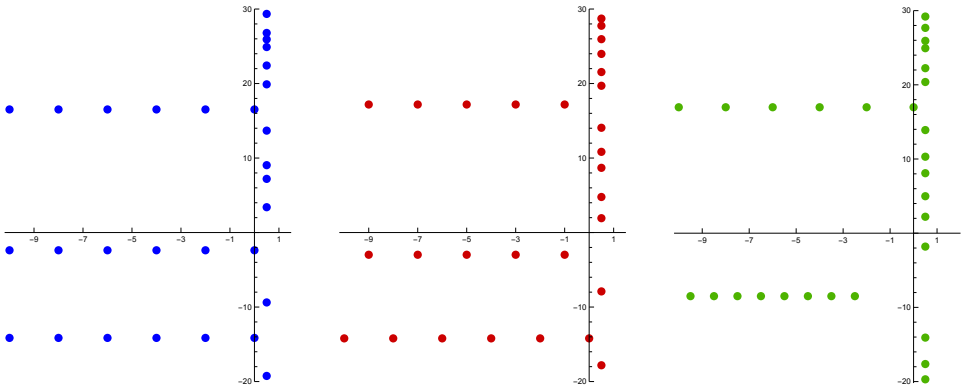

FIGURE 4.2. The zeros in the complex s-plane of the L-functions in Figure 4.1, now presented from left to right. In the region shown, the nontrivial zeros all lie on the critical line $\mathrm{Re}(s) = \frac{1}{2}$.

4.2. The explicit formula explains zero-free intervals. The pushing-aside phenomenon was first observed in [**24**]. As shown by [**2**] it can be rigorously established using Weil's explicit formula. This formula in cartoon form says

$$\sum_{\gamma} f(\gamma) = \hat{f}(0) \cdot (\log N) + \int f(t) \frac{\Gamma'}{\Gamma}\text{-terms}\, dt + \sum_{n} \hat{f}\big(\frac{\log n}{2\pi}\big)\text{coeffs.} \tag{4.1}$$

Here f is a test function, $\hat{f}$ is its Fourier transform, N is the conductor of the given L-function, and the sum on the left is over the zeros. The argument in [**2**] chooses f to be non-negative, so the left side of (4.1) can be interpreted as the weighted count of the zeros within the support of f. The test function is chosen to have support in an interval I containing the heights of the trivial zeros in question. Here the Γ'/Γ terms on the right are negative, the effect being stronger when the zeros are closer to the critical line. In this way, with the conductor small enough as well, one can prove certain intervals I indeed contain no zeros.

4.3. The explicit formula and the approximate functional equation explain L-point-free regions. A striking feature of Figures 3.1, 3.2, and 3.3 is that there are no L-points in certain large regions. Such an L-point-free region was established for the case of Figure 3.1 in [**20**] using the explicit formula (4.1). The L-point-free region was enlarged in [**6**] by using the approximate functional equation (3.4). See Figure 1 in [**6**].

The basic idea behind the proof in [**20**] is that for a point (λ_1, λ_2) in the region in question one can choose a test function f taking only nonnegative values in (4.1) so that the right side of (4.1) is negative. But the left side of (4.1) is nonnegative and the conclusion is that no L-function with coordinates at (λ_1, λ_2) can exist. This same general method has been applied in many contexts. For example, simply taking $(\lambda_1, \lambda_2) = (0, 0)$ one is saying that certain L-functions coming from number fields can only exist if conductors are large enough [**13**]. The method, and the more powerful exclusionary techniques of [**6**], can be extended to establish L-point-free regions of other landscapes.

For the discussion in §6.5 and §6.6 we are interested in how the L-point-free region varies with the parameter space. For example, consider the two different parameter spaces which are superimposed in Figure 3.3, for which the Plancherel measures are exactly the same. Observationally, the lowest points on lines where κ is integral are lower than the lowest points on lines where κ is half-integral. Accordingly, we expect a larger zero-free region in X_{+c} than in X_{-c}. From the viewpoint of the explicit formula, the situation is similar to the contrast between the three cases in Figure 4.2. Namely the factor $\Gamma_{\mathbb{R}}(s + i\lambda)$ gives a larger negative contribution to the Γ'/Γ-term in (4.1) than the factor $\Gamma_{\mathbb{R}}(s + 1 + i\lambda)$ does.

5. Coefficient space

Here we treat general degrees d and explain how the union X'_d of all the connected parameter spaces X'_{d_+,d_-,d_2} maps finite-to-1 to a single ***coefficient space*** $Y'_d = \mathbb{R}^{d-1}$. Information is lost, because of the failure of injectivity, but many parameter landscapes, like Figures 3.1, 3.2, and 3.3 are combined into a single coefficient landscape, like Figure 5.2.

5.1. Spectral parameters as three multisets of complex numbers. An equivalent way to give spectral parameters is to give multisets Z_+, Z_-, and Z_2 of complex numbers in a slightly different way, as follows:

$$\begin{aligned}
\Gamma_{\mathbb{R}}(s + i\lambda) &\text{ contributes } \lambda \text{ to } Z_+,\\
\Gamma_{\mathbb{R}}(s + 1 + i\lambda) &\text{ contributes } \lambda \text{ to } Z_-, \text{ and}\\
\Gamma_{\mathbb{C}}(s + \kappa + i\lambda) &\text{ contributes } \lambda + i\kappa \text{ and } \lambda - i\kappa \text{ to } Z_2.
\end{aligned}$$

We call the triple (Z_+, Z_-, Z_2) a **dot diagram** because we think of it visually as illustrated by Figure 5.1. So the space X_d of allowed spectral parameters in degree d is identified with the space of dot diagrams having d dots, counting multiplicities. Repeating material from §2.5 in the new language, X_d decomposes as the disjoint union of the subspaces X_{d_1,d_2} parameterizing dot diagrams with d_2 complex conjugate pairs of non-real roots. Each X_{d_1,d_2} then decomposes into the disjoint union of the subspaces X_{d_+,d_-,d_2} parametrizing dot diagrams with $|Z_+| = d_+$, $|Z_-| = d_-$, and $|Z_2| = 2d_2$. To understand the previously-defined topology of all these spaces one should think of the dots as being allowed to move horizontally in the complex plane. Dots are allowed to cross and dots of a given type are indistinguishable. The ambient spaces X'_d introduced in §2.5 correspond to letting complex conjugate pairs of dots move arbitrarily in $\mathbb{C} - \mathbb{R}$.

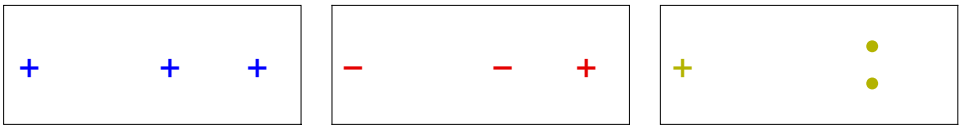

FIGURE 5.1. Dot diagrams, drawn left to right, for the Γ-factors of Figure 4.1, drawn in the rectangle with $|\mathrm{Re}(z)| \leq 20$ and $|\mathrm{Im}(z)| \leq 8$.

The viewpoint on the X_{d_+,d_-,d_2} of the previous sections of course remains valid. Thus, as explained before, the closed yellow cones in Figures 3.1 and 3.2 respectively indicate half of $X_{3,0,0} = X_{+++}$ and $X_{1,2,0} = X_{+--}$. Likewise one should think of Figure 3.3 as a picture of the upper half of both $X_{+c} \subset X'_{+c}$ and $X_{-c} \subset X'_{-c}$, as each full space $X_{\tau c}$ has the form $\frac{1}{2}\mathbb{Z}_{\geq 1} \times \mathbb{R}$.

5.2. Spectral parameters as factorizing real polynomials. Our introduction of coordinates $(\lambda_1, \ldots, \lambda_{d_1-1})$ and $(\kappa_1, \ldots, \kappa_{d_2})$ on X'_{d_1,d_2} in §2.5 involved an ordering convention from §2.2. As is often the case, it is good to have convention-independent coordinates. Accordingly, we form corresponding monic polynomials,

$$f_\epsilon(x) = \prod_{z \in Z_\epsilon} (x - z) \in \mathbb{R}[x]. \tag{5.1}$$

The distinction between the + points and the − points plays a secondary role, and so it is moreover useful to consider the product,

$$f(x) = f_+(x) f_-(x) f_2(x) = x^d + c_2 x^{d-2} + \cdots + c_{d-1} x + c_d. \tag{5.2}$$

Thus a point (Z_+, Z_-, Z_2) of X'_d determines a point $(c_2, \ldots, c_d)$ of $\mathbb{R}^{d-1}$. The dual of (Z_+, Z_-, Z_2) is $(-Z_+, -Z_-, -Z_2)$. In the new coordinates, dualizing corresponds to replacing $f(x)$ by $(-1)^d f(-x)$ so that c_j is replaced by $(-1)^j c_j$.

Let $Y_d \subset \mathbb{R}^{d-1}$ be the image of X_d and let Y_{d_1,d_2} be the image of X_{d_1,d_2}. The map $X_{d_1,d_2} \to Y_{d_1,d_2}$ corresponds to forgetting the distinction between the + and − points. It is thus a branched cover of degree 2^{d_1}. Numerics are governed by a row of Pascal's triangle, as the branched cover $X_{d_+,d_-,d_2} \to Y_{d_1,d_2}$ has degree the binomial coefficient $\frac{d_1!}{d_-!d_+!}$. These numerics stay the same if we consider the enlarged spaces X'_{d_+,d_-,d_2} and their images Y'_{d_1,d_2}.

5.3. The coefficient landscape. Figure 5.2 draws a window on the upper half of the coefficient plane $Y_3' = \mathbb{R}^2$. Also included are the data points from Figures 3.1, 3.2, 3.3, and their duals. The space $Y_{3,0}$ is the subspace where the discriminant $D = -27c_3^2 - 4c_2^3$ is positive or zero. It is filled by blue points coming from the bijection $X_{+++} \to Y_{3,0}$ and red points from the triple cover $X_{+--} \to Y_{3,0}$.

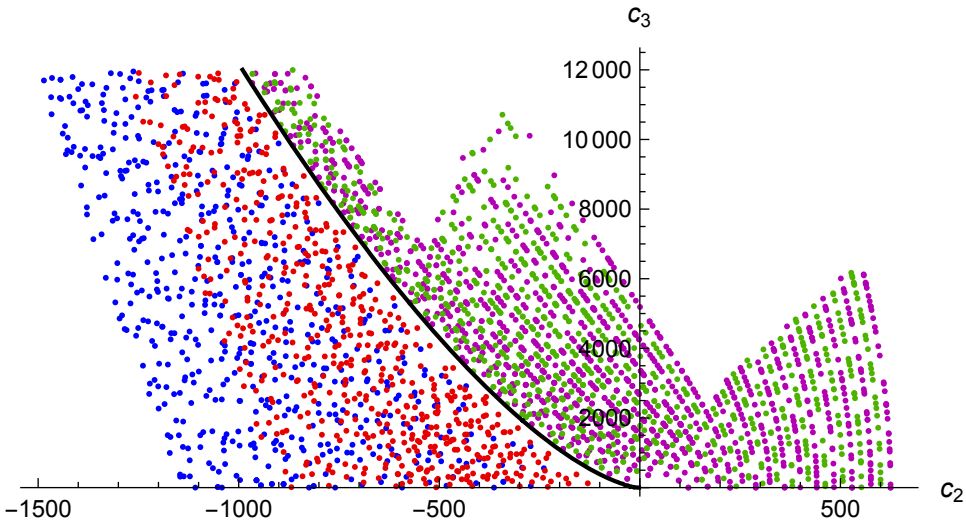

FIGURE 5.2. Landscape of L-functions in the coefficient plane $Y_3' = \mathbb{R}^2$.

For a real number κ, let C_κ be the contour curve with equation $D = -4\kappa^6$, so that C_0 is the drawn discriminant locus bounding $Y_{3,0}$. The space $Y_{1,1}$ is a union of curves C_κ indexed by $\kappa \in \frac{1}{2}\mathbb{Z}_{\geq 1}$. The maps from X_{-c} and X_{+c} to $Y_{1,1}$ are both bijective. The curve C_κ contains purple points from X_{-c} or green points from X_{+c}, according to whether κ is an integer or not.

A key feature of Figure 5.2 and also Figure 6.2 is a decomposition of $\mathbb{R}^{d-1}$ into two regions via the discriminant D, a left one where $D \geq 0$ and a right one where $D < 0$. In the general case, there are $\lceil d/2 \rceil$ parts, the images of the X'_{d_1,d_2}. All the components of Y_d are entirely inside one of these parts. The components of Y_d in the image of X'_{d_1,d_2} all have codimension d_2.

6. Plancherel measure

In the parts near the origin, where data should be at least nearly complete, there is a noticeable difference between the varying density of L-points in parameter spaces, as illustrated by Figures 3.1, 3.2, and 3.3, and the more uniform density of L-points in coefficient space, as illustrated by Figure 5.2. Here we explain how Plancherel measure gives a clear theoretical framework which in particular explains the visual difference.

6.1. The global meaning of Plancherel measure. Plancherel measure is naturally defined via the group $\mathrm{GL}_d(\mathbb{R})$ and plays a large role in many purely local questions. However, we are interested in this paper only in its conjectural role in

counting L-functions and so will take a more global viewpoint. For a measurable set $U \subset X_d$ and a positive integer N, let $\mathcal{L}(U, N)$ be the set of L-functions with Γ-factor in U and conductor N. Then the governing principle is that one should have

$$|\mathcal{L}(U, N)| \approx \mu_d(U)\nu_d(N), \tag{6.1}$$

for a multiplicative function ν_d on positive integers coming from analogous Plancherel measures for the p-adic groups $\mathrm{GL}_d(\mathbb{Q}_p)$. Rigorously, one conjectures an asymptotic equivalence as the cutoff x goes to infinity,

$$\sum_{N \le x} |\mathcal{L}(U, N)| \sim \sum_{N \le x} \mu_d(U)\nu_d(N). \tag{6.2}$$

The general asymptotic equivalence (6.2) can only hold for at most one pair of measures, so (6.2) is in particular a conjectural global characterization of the Plancherel measure μ_d. Theorem 1 of [**14**], with a special case given in (6.6) below, is one of many strong statements in the literature supporting the general truth of (6.2).

As a simple illustration of this formalism, let $d = 1$ where $X_1 = X_+ \sqcup X_-$. Each summand on the right has one element and maps bijectively to $Y_1 = \{0\} = \mathbb{R}^0$. The number $\nu_1(p^j)$ is the number of characters $(\mathbb{Z}/p^j)^\times \to \mathbb{C}^\times$ that do not factor through the quotient group $(\mathbb{Z}/p^{j-1})^\times$. Thus, e.g., $\nu_1(p) = p - 2$ for any prime p. To give a primitive Dirichlet character $\chi : (\mathbb{Z}/N)^\times \to \mathbb{C}^\times$ with $N = \prod_p p^{e_p}$ is to give an injective character $\chi_p : (\mathbb{Z}/p^{e_p})^\times \to \mathbb{C}^\times$ for each p. For $N \ge 2$ the two possible values 1 and -1 arise equally often for $\chi(-1)$. The Plancherel measure μ_1 gives mass $1/2$ to both X_+ and X_-. So in fact (6.1) holds as an equality for all U and all $N \ge 2$. The behavior at $N = 1$ represents a doubling phenomenon which holds for all d: half the Γ-factors are excluded and the others should asymptotically occur at twice their Plancherel density.

6.2. Modified absolute values and near-constant densities. This subsection and the next are essentially translations of presentations in the literature into more intuitive terms. See, e.g., [**11**] for a more Lie-theoretic presentation. As a preliminary for writing down Plancherel measures on parameter spaces X_{d_1,d_2} in an intuitive way, define

$$|t|_+ = t \tanh\Big(\frac{\pi}{2}t\Big), \qquad |t|_- = t \coth\Big(\frac{\pi}{2}t\Big), \qquad |t|_0 = |t|.$$

To help understand Plancherel measures on coefficient spaces Y_d, restrict to $t \ge 0$ and consider the change of variables $s = t^2$, and thus $t = s^{1/2}$ and $dt = \frac{1}{2}s^{-1/2}ds$. Then the differential form $tf(t)dt$ is equal to $s^{1/2}f(s^{1/2})\frac{1}{2}s^{-1/2}ds = \frac{1}{2}f(s^{1/2})ds$.

Figure 6.1 shows that $|t|_+$ has a double-zero at $t = 0$ while $|0|_- = 2/\pi$. This distinction is important when comparing with data for large N, but in our context of $N = 1$ it is negligible, as we will discuss further. More important to us is the fact, obvious from the defining formulas, that the modifications $|t|_\epsilon$ each approach $|t|$ exponentially fast as $|t| \to \infty$. So the corresponding densities in the s-variable likewise converge rapidly to $1/2$.

6.3. Plancherel measure and its near-Euclidean nature. For constants P_d specified in the next subsection, the Plancherel measure is given on the $(d_1 +$

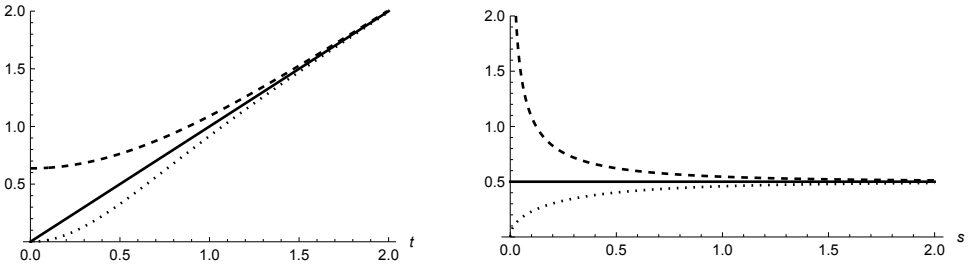

FIGURE 6.1. Left: densities $|t|_+$ (dotted), $|t|_-$ (dashed), and $|t|_0 = |t|$ (solid). Right: associated densities $\tanh(\pi\sqrt{s}/2)/2$, $\coth(\pi\sqrt{s}/2)/2$, and $1/2$.

$d_2 - 1$)-dimensional part X_{d_1,d_2} of X_d by

$$\mu_d = \frac{P_d}{2^{d_1+d_2}} \prod_{i<j} |z_i - z_j|_{\epsilon_i\epsilon_j} \; d\lambda_1 \cdots d\lambda_{d_1+d_2-1}. \tag{6.3}$$

Here the z_i run over the points in the dot diagram and ϵ_i is $+$, $-$ or 0 according to whether z_i is in Z_+, Z_-, or Z_2. The factor 2^{d_1} in the denominator arises from the previously mentioned fact that the map from X_{d_1,d_2} to its image Y_{d_1,d_2} has degree 2^{d_1}. The factor 2^{d_2} goes away in (6.4) because each of the κ_i are allowed to be $\frac{1}{2}\mathbb{Z}_{\geq 1}$, rather than just in $\mathbb{Z}_{\geq 1}$.

Formula (6.3) lets one supplement the vision of moving dots in diagrams such as Figure 5.1: the dots tend to repel each other in the sense that moving any two dots further apart contributes to an increase in Plancherel density. At close range, the distinction between the subscripts $+$, $-$, and 0 is important, but at long range it is not.

In our cases in the setting $d = 3$, using $\lambda_1 + \lambda_2 + \lambda_3 = 0$ in the first two cases, (6.3) becomes these more explicit formulas:

$$\text{on } X_{+++}, \qquad \mu_3 = \frac{P_3}{8} |\lambda_1 - \lambda_2|_+ \, |2\lambda_1 + \lambda_2|_+ \, |\lambda_1 + 2\lambda_2|_+ \, d\lambda_1 \, d\lambda_2,$$

$$\text{on } X_{+--}, \qquad \mu_3 = \frac{P_3}{8} |\lambda_1 - \lambda_2|_- \, |2\lambda_1 + \lambda_2|_+ \, |\lambda_1 + 2\lambda_2|_- \, d\lambda_1 \, d\lambda_2,$$

$$\text{on } X_{-c} \text{ and } X_{+c}, \qquad \mu_3 = \frac{P_3}{8} \kappa(4\kappa^2 + 9\lambda^2) \, d\lambda.$$

The first two densities are indicated by light contour plots in the background in Figures 3.1 and 3.2 respectively, where they are nearly indistinguishable except near the line $\lambda_1 = \lambda_2$, where only one of the measures vanishes. Although the third measure is supported on a union of vertical lines in Figure 3.3, the background there nonetheless gives the contour plot of $\kappa(4\kappa^2 + 9\lambda^2)$ on the entire positive quadrant.

Now consider the enlarged parameter spaces X'_d obtained by allowing each κ_j to run over $(0, \infty)$ as discussed before. On each piece X'_{d_1,d_2} define

$$\mu'_d = \frac{P_d}{2^{d_1}} \prod_{i<j} |z_i - z_j| \; d\lambda_1 \cdots d\lambda_{d_1+d_2-1} \, d\kappa_1 \cdots d\kappa_{d_2}. \tag{6.4}$$

A standard fact about discriminants, explained in [**12**] for example, then says that the push-forward of μ'_d to coefficient space $\mathbb{R}^{d-1}$ via (5.1) and (5.2) is just the

Euclidean measure $P_d\, dc_2 \dots dc_d$. Keeping in mind that the differences between the three $|t|_\epsilon$ decay exponentially as t becomes large, as illustrated by Figure 6.1, and our root distances are almost always large, as illustrated by Figure 5.1, the conclusion is that Plancherel measure on coefficient space is extremely close to a Euclidean measure for our purposes.

6.4. Plancherel constants. To get the global constant P_d, we compare the main theorem of [**14**], as made explicit by [**10**], with a much more elementary result from [**12**].

Laplacian asymptotics. The Laplacian eigenvalue associated to an automorphic L-function with $(d_1, d_2) = (d, 0)$ and spectral parameters $(\lambda_1, \dots, \lambda_d)$ in the conventions of [**14**] is

$$\Lambda = 1 + \frac{\lambda_1^2 + \cdots + \lambda_d^2}{2}. \tag{6.5}$$

Placing an instance of $|\mathcal{L}(U, 1)|$ from (6.1) in the notation of [**14**], let $N(T)$ be the number of such L-functions with conductor $N = 1$ and Laplacian eigenvalue $\Lambda \le T$. The symmetric space $M = K \setminus \mathrm{PGL}_d(\mathbb{R})/\mathrm{PGL}_d(\mathbb{Z})$ has dimension $m = \sum_{j=2}^d j = (d+2)(d-1)/2$. Theorem 1 of [**14**], specialized to the group $\mathrm{PGL}_d(\mathbb{R})$, gives the asymptotic

$$N(T) \sim \frac{\mathrm{vol}(M)}{\Gamma(\frac{m}{2}+1)(4\pi)^{m/2}} T^{m/2}. \tag{6.6}$$

Here the volume depends on the ratio of choices of Haar measure for $\mathrm{PGL}_d(\mathbb{R})$ and K. With the choices described in [**14**, Section 3], the volume is calculated in [**10**, Theorem 1.6.1] as

$$\mathrm{vol}(M) = \frac{d}{\pi^{m/2}} \prod_{j=2}^{d} \zeta(j) \Gamma\Big(\frac{j}{2}\Big). \tag{6.7}$$

A Euclidean volume. On the other hand, the part $Y_{d,0}^r$ of coefficient space $\mathbb{R}^{d-1}$ coming from $(\lambda_1, \dots, \lambda_d)$ with $\lambda_1^2 + \cdots + \lambda_d^2 \le r^2$ is just the part of $Y_{d,0}$ with $c_2 \ge -r^2/2$. For example the upper half of $Y_{3,0}^{\sqrt{2000}}$ is the part of Figure 5.2 beneath the drawn discriminant curve C_0. The Euclidean volume of $Y_{d,0}^r$, with respect to the measure $dc_2 \cdots dc_d$, is calculated via a Selberg integral in [**12**, Props. 1.1 and 1.2] to be

$$\mathrm{vol}(Y_{d,0}^r) = \frac{\prod_{j=2}^d \Gamma(\frac{j}{2})}{2^{d(d-1)/4}\sqrt{d}\,\Gamma(\frac{m}{2}+1)} r^m. \tag{6.8}$$

Note that the right sides of (6.6), (6.7), and (6.8) all have a slightly different form from the right sides in the references. We have made these small changes, using facts like the duplication formula for the Γ-function, so as to make the simplification (6.9) short.

Comparison. If we replaced T on the right side of (6.6) by $T - 1$, the asymptotic would still be true. So, the desired Plancherel constant P_d is the ratio of the right

sides of (6.6) and (6.8), with T replaced by $r^2/2$ in conformity with (6.5):

$$\begin{aligned} P_d &= \frac{\frac{d}{\pi^{m/2}}\prod_{\ell=2}^{d}\zeta(\ell)\Gamma(\frac{\ell}{2})}{\Gamma(\frac{m}{2}+1)(4\pi)^{m/2}}(r^2/2)^{m/2}\cdot\frac{2^{d(d-1)/4}\sqrt{d}\Gamma(\frac{m}{2}+1)}{\prod_{j=2}^{d}\Gamma(\frac{j}{2})}r^{-m} \\ &= \frac{\frac{d}{\pi^{m/2}}\prod_{\ell=2}^{d}\zeta(\ell)}{(4\pi)^{m/2}}2^{-m/2}\cdot 2^{d(d-1)/4}\sqrt{d} \\ &= \frac{d^{3/2}}{2^{(d+3)(d-1)/2}}\prod_{j=2}^{d}\frac{\zeta(j)}{\pi^j}. \end{aligned} \tag{6.9}$$

The final formula is written so that the factor $\zeta(j)/\pi^j$ is rational for even j. Special cases of (6.9) are $P_1 = 1$, $P_2 = \frac{1}{12}$ and the evaluation (1.2) of P_3 highlighted in the introduction.

6.5. Comparison of data and theory in $d = 2$. In this subsection and the next, we compare three things: computed data, Plancherel measure μ_d, and the Euclidean approximation μ_d' to Plancherel measure. Here we summarize the well-understood $d = 2$ case, using it to calibrate our expectations for our $d = 3$ case.

We are guided in the $d = 2$ case by Figure 6.2, which is to be compared with Figure 5.2 for the $d = 3$ case. The Euclidean approximation $\mu_2' = \frac{dc_2}{12}$ gives mass 50 to both the intervals $[-600, 0]$ and $[0, 600]$. But, as indicated by the colored L-points, taken from [**16**], there are only 19 L-functions in the negative half, giving the very low percentage 38%. For the positive half, write always $k = 2\kappa + 1$ and thus $\kappa = (k-1)/2$. An L-point at $\kappa \in \frac{1}{2}\mathbb{Z}_{\geq 1}$ arises with multiplicity the dimension of the space of cusp forms $S_k(1)$ of weight k on $\mathrm{SL}_2(\mathbb{Z})$. For odd k, this dimension is always 0. For $k = 12$, 14, 16, 18, 20, and 22 the dimensions are 1, 0, 1, 1, 1, and 1. Adding 12 to an even k increases the multiplicity by 1, for a general approximate formula of $(k-1)/12$. These multiplicities are indicated by the areas of the L-points, with the rightmost drawn L-point coming from $k = 48$ and its multiplicity of 4. The total number of L-points, including multiplicity, works out to 37, for the still small percentage of 74%. So we are interested here in obtaining some understanding of why these percentages are so small.

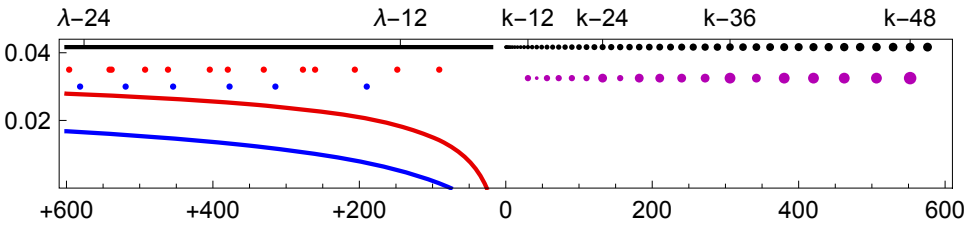

FIGURE 6.2. Plancherel measure on the c_2-interval $[-600, 600]$ indicated in black at the top. Colored L-points come from Maass forms on the left and holomorphic cusp forms on the right.

For $c_2 > 0$, it is helpful to use the function $f(k) = ((k-1)/2)^2$. Plancherel measure is supported on $f(\mathbb{Z}_{\geq 2})$. By the case of (6.3) with no differentials it gives

mass $(k-1)/24$ to $f(k)$. A natural cutoff is $C = f(K+1/2)$ for a positive integer K. Then, assuming that K is a multiple of 12 for the last formula,

$$\mu_2'([0,C]) = \frac{f(K+1/2)}{12} = \frac{K^2}{48} - \frac{K}{48} + \frac{1}{192}, \tag{6.10}$$

$$\mu_2([0,C]) = \sum_{k=2}^{K} \frac{k-1}{24} = \frac{K^2}{48} - \frac{K}{48}, \tag{6.11}$$

$$|\mathcal{L}([0,C],1)| = \sum_{k=2}^{K} \dim(S_k(1)) = \frac{K^2}{48} - \frac{14K}{48} + \frac{244}{192}. \tag{6.12}$$

So the low-percentage problem is not a failure of μ_2' to be a good approximation for μ_2. One can rewrite the discrepancy between the theories (6.10), (6.11) and the data (6.12) in the c_2 variable. One then gets that for $c_2 > 10$ the density

$$f_c(c_2) = \frac{1}{12}\left(1 - \frac{3.25}{\sqrt{c_2}}\right) \tag{6.13}$$

approximates the density of L-points much better than $\frac{1}{12}$ does. Note also that the doubling phenomenon arises here: at level $N = 1$, odd k never occur and so even k occur twice as often as Plancherel measure would predict.

For $c_2 < 0$ there is still a doubling phenomenon: at level $N = 1$, dot diagrams of the form $+-$ cannot occur and so $++$ and $--$ asymptotically occur twice as often as Plancherel measure would predict. So both $++$ and $--$ should have asymptotic average density $1/24$. This exact constant comes from the Euclidean measure μ_2' and is graphed in Figure 6.2. The density for actual Plancherel measure μ would visually differ from $1/24$ only in the c_2 interval $[-2, 0]$, by the asymptotic constancy of the right half of Figure 6.1. Five-term refinements for the counting functions with a very small error terms are given in [**23**, Eqs. 40,41]. Taking only three terms, the corresponding densities written in terms of $b = |c_2|$ are

$$f_{++}(b) = \frac{1}{24}\left(1 - \frac{9\log(b) + 3\log(\pi^4/2)}{\pi\sqrt{b}}\right), \tag{6.14}$$

$$f_{--}(b) = \frac{1}{24}\left(1 - \frac{3\log(b) + 3\log(8)}{8\pi\sqrt{b}}\right). \tag{6.15}$$

These functions are plotted in Figure 6.2. Their low values over the plotted region are consistent with there being only 6 L-functions of type $++$ and 13 L-functions of type $--$, rather than the 25 of each that Plancherel measure alone would predict. The slow approach of these functions to their common asymptote is illustrated by the numerical values $24f_{++}(10000) \approx 77\%$ and $24f_{--}(10000) \approx 89\%$.

6.6. Comparison of data and theory in $d = 3$. We can now compare the coefficient landscape drawn in Figure 5.2 with expectations from theory. The Plancherel measure of any rectangle of size say 200-by-2000 is almost exactly $(200)(2000)P_3 \approx 210$. From the previous subsection, we should not expect to obtain this density in the range of the figure, but we should expect to be closer in the region with $d_1 = 1$ to the right than we are in the region with $d_1 = 3$ to the left. A greater density is indeed visually apparent on the right. For example, the rectangle with $-300 \le c_2 \le -100$ and $2000 \le c_3 \le 4000$ has 134 green and purple L-points, giving the percentage $134/210 \approx 64\%$. In comparison, the rectangle with

$-500 \le c_2 \le -300$ and $0 \le c_3 \le 1000$ in the totally real region on the left has only 90 blue and red L-points, which is about 43% of 210.

We think it is possible that we have found almost all the L-points in the two sample rectangles just mentioned. If one goes closer to $(c_2, c_3) = (0, 0)$, we think it is more likely that we have found all the L-functions. Here the percentages are generally lower, and we interpret that as being from secondary effects, capturing not only that there are no L-points in the L-point-free regions discussed in §4.3, but that L-points close to these regions should be sparse. If one goes further from $(c_2, c_3) = (0, 0)$ again the experimental density tends to decrease, but now it is clear that our searches have simply missed L-functions.

In interpreting the difference between the blue L-points from X_{+++} and the red L-points from X_{+--} on the totally real side, one needs to keep in mind that there are asymptotically three times as many of the latter as there are of the former. But even with this in mind, the data near the discriminant locus C_0 suggests that secondary effects for $+++$ are much stronger than they are for $+--$; this is expected from comparison of the $++$ and the $--$ cases in $d = 2$. More data would be very helpful in making a more detailed analysis. Even more helpful would be refined densities with more terms, analogous to (6.13), (6.14), and (6.15).

7. Complements

We conclude by pointing to two promising future directions. We describe them briefly here. Both involve the partially conjectural concept of the Sato-Tate group associated to an L-function.

7.1. Comparison with the p-adic Plancherel formula. Another way to examine our collection of L-functions is to compare it with expectations from the spherical p-adic Plancherel formula. This formula asymptotically governs the distribution of coefficients $a_p \in \mathbb{C}$ for a fixed prime p and varying L-functions. There are uniform formulas for all d, but we will be briefer than in the last section and consider only our case $d = 3$.

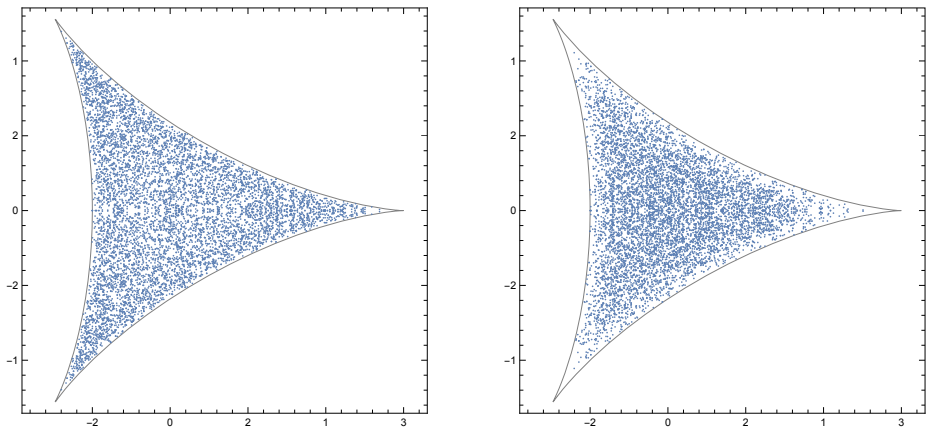

FIGURE 7.1. Coefficients a_p from the degree 3 conductor 1 L-functions in our collection: a_2's on the left and a_5's on the right.

To see some data before bringing in theory, Figure 7.1 plots the a_2's and a_5's of all the degree 3 conductor 1 L-functions in our collection, a total of 8564 examples. The reflection symmetry across the real-axis comes from duality of L-functions. The Ramanujan conjecture says that each a_p should agree with the trace of an element of the compact group SU_3. The conjecture holds here, as expected, because the a_p indeed lie in the curvilinear triangle T of traces. Writing the generic element in the complex plane as $z = x + iy$, the boundary of T is given by the vanishing of

$$f(x, y) = 27 - 18x^2 + 8x^3 - x^4 - 18y^2 - 24xy^2 - 2x^2y^2 - y^4.$$

For a fixed non-self-dual L-function and varying p, the a_p are conjectured to be equidistributed in T according to the push-forward of the Haar measure on SU_3. The density of this Sato-Tate measure $\mu_\infty = f_\infty(x, y)dxdy$ works out to $f_\infty(x, y) = \sqrt{f(x, y)}/(2\pi^2)$.

The p-adic Plancherel measures $\mu_p = f_p(x, y)dxdy$ fit together to form a family indexed by $p \in [1, \infty]$, with $p = \infty$ giving the Sato-Tate measure just discussed. The density $f_1(x, y)$ is constant. The formula for general p is too complicated to give here, but for $p > 1$ all the $f_p(x, y)$ vanish on the boundary, and the unique maximum is at $(0, 0)$ and increases with p. A precise statement which captures this phenomenon of increasing concentration in the middle is

$$\int_T f_p(x, y)(x^2 + y^2)dxdy = 1 + \frac{1}{p} + \frac{1}{p^2}. \tag{7.1}$$

We obtained all these statements by specializing the general definition of p-adic Plancherel measure [**17**] to SU_3 and then carrying out the requisite multivariate calculus.

Figure 7.1 shares qualitative features with the behavior predicted by p-adic Plancherel measures. For example, the distribution of the a_2's is hard to visually distinguish from the uniform distribution, but the distribution of the a_5's already shows marked repulsion from the boundary. However, quantitatively, experimental moments are far off from theoretical moments:

p	2	3	5
Theoretical moment from (7.1)	1.75	1.44	1.24
Experimental moment from dataset	1.47	1.12	0.93

We again expect that this discrepancy is explained by as yet unknown secondary terms.

7.2. Group-theoretical framework. To make our concrete points in the next two subsections cleanly, we first bring in more formalism. To understand the full set $\mathcal{L}$ of all automorphic L-functions it is clarifying to use the conjectural ***Langlands group*** G and two of its quotients:

$$G \twoheadrightarrow G^{\mathrm{alg}} \twoheadrightarrow G^{\mathrm{fin}}. \tag{7.2}$$

Here G is a very large compact group containing Frobenius classes Fr_p for all primes p. The set of irreducible representations of G is identified with $\mathcal{L}$ by requiring that a representation ρ corresponding to an L-function $L(s) = \prod_p f_p(p^{-s})^{-1}$ satisfy $f_p(x) = \det(1 - \rho(\mathrm{Fr}_p)x)$ for all primes p not dividing the conductor. The representations that factor through G^{alg} correspond to L-functions in $\mathcal{L}^{\mathrm{alg}}$, therefore L-functions for which the λ_j are all 0. The representations that factor through

G^{fin} correspond to L-functions for which the κ_k are also all 0, equivalently, there are no $\Gamma_{\mathbb{C}}$ in our normalization of the Γ-factors. Conjecturally, G^{alg} has an independent definition as a compact version of the absolute motivic Galois group of $\mathbb{Q}$. Conjecturally, $G^{\text{fin}} = \text{Gal}(\overline{\mathbb{Q}}/\mathbb{Q})$. The ***Sato-Tate group*** of an L-function L is the image of the corresponding representation ρ; it is a compact subgroup of $\text{GL}_d(\mathbb{C})$, well-defined up to conjugation. In general Frobenius elements are conjectured to be equidistributed in the conjugacy classes of the Sato-Tate group, as mentioned in the previous subsection for the Sato-Tate group SU_3.

If the Sato-Tate group of an L-function has c components, then the component group conjecturally comes from a Galois number field of degree c. Any prime dividing the discriminant of this field divides the conductor of the L-function. So requiring $N = 1$ forces Sato-Tate groups to be connected. Also the abelianizations of the three groups (7.2) are expected to coincide with the abelianization $\hat{\mathbb{Z}}^{\times}$ of $\text{Gal}(\overline{\mathbb{Q}}/\mathbb{Q})$. So, at $N = 1$, tori are also ruled out as possible Sato-Tate groups.

For $d = 3$ and $N = 1$ there are only two possibilities. The Sato-Tate group is SO_3 in the special case that the L-function is self-dual and SU_3 otherwise. This simple dichotomy allowed us to ignore the group-theoretical framework in previous sections. But when one allows general N, there are infinitely many possible G, with the finite groups arising in §3.4 illustrating some possibilities. To regain some simplicity in discussing the landscapes for (d, N), one can focus on ***generic*** L-functions. By definition, these are L-functions whose Sato-Tate groups contain SU_d, with d being the degree. One expects that for any fixed d, 100% of L-functions are generic asymptotically, for say a ball centered at the origin in coefficient space $\mathbb{R}^{d-1}$ of increasing radius.

7.3. Generic algebraic L-functions are hard to find for $d \geq 3$. We now support a main theme of the introduction, that algebraic L-functions are relatively rare for degrees $d \geq 3$. The classical degrees do not point in the right direction at all: in degree 1, all L-functions are algebraic. For $d = 2$, an L-function is algebraic if and only if $c_2 \geq 0$ as illustrated by Figure 6.2; so Plancherel measure says in a strong sense that half of the L-functions are algebraic and half are not.

The set Y_3^{alg} is just the set of points $(c_2, c_3) = (\kappa^2, 0)$ for $\kappa \in \mathbb{Z}_{\geq 0}$. We impose genericity for the rest of this subsection, thereby excluding the parameter $\kappa = 0$. Computations with the cohomology of $\text{SL}_3(\mathbb{Z})$ in [**1**] say that there are no generic L-functions in $\mathcal{L}_{3,1}^{\text{alg}}$ with $N = 1$ and $\kappa < 120$. To see some algebraic L-functions, we increase the conductor, like we did in §3.4. At $\kappa = 1$, cohomological computations with congruence subgroups in [**25**] show the existence of dual pairs of generic L-functions for the conductors 89, 106, 116, 128, 160, 205, 212, and 221. An L-function with L-point $(\kappa^2, 0)$ for $\kappa \in \mathbb{Z}_{\geq 1}$ should come from a motive with nonvanishing Hodge numbers $h^{2\kappa,0} = h^{\kappa,\kappa} = h^{0,2\kappa} = 1$. For $\kappa = 1$, a one-parameter family of such motives was found in the cohomology of surfaces in [**26**]. A dual pair of members of this family numerically matches the dual pair of automorphic L-functions with conductor 128. For $\kappa > 1$ there is a qualitative difference, as Griffiths transversality prevents motives from moving in families, and so algebraic geometry can only produce them one dual pair at a time.

In summary, generic algebraic L-functions in degree $d = 3$ are known only for $\kappa = 1$. For $d \geq 4$, the only examples we know of come from families of threefolds in [**5**, **22**], with nonvanishing Hodge numbers $h^{3,0} = h^{2,1} = h^{1,2} = h^{0,3} = 1$; the

smallest conductor seems to be $2^9 3^9$, so matching automorphic calculations are out of reach.

7.4. Comparison in the self-dual setting. For a more subtle comparison, consider now only L-functions in $\mathcal{L}$ with real coefficients. According to the group-theoretic framework, they come in two types, orthogonal and symplectic, the latter arising only for d odd. In the spirit of the Frobenius-Schur indicator, we use $\tau \in \{+, -\}$ to distinguish them, with $+$ for orthogonal and $-$ for symplectic.

The theoretical context set up in this paper has direct analogs in both of these two parallel settings. Thus there are sets of L-functions $\mathcal{L}^{\tau}_{d,N}$ mapping to disconnected parameter spaces X^{τ}_{d} of possible Γ-factors which in turn map to coefficient spaces $Y^{\tau}_{d} \subset \mathbb{R}^r$. Here $r = \lfloor d/2 \rfloor$ arises as the dimension of a maximal torus in the compact group Sp_d or O_d. There is again a Plancherel measure μ_τ on Y^{τ}_{d} and again a canonical Euclidean approximation μ'_τ on $\mathbb{R}^r$. Again μ_τ should govern the distribution of L-points. A difference is that Y^{τ}_{d} contains components of all the possible dimensions $0, \ldots, r$. So Figure 6.2 for $\mathrm{SU}_2 = \mathrm{Sp}_2$ is a good guide. Like in the $d = 2$ case, the isolated points are algebraic and each has positive Plancherel measure. Another difference is that algebraic geometry provides many large families of source motives for the algebraic points of many of the larger-dimensional components. For example, the $g(g+1)/2$-dimensional family of dimension g abelian varieties maps to the algebraic point of a $\lfloor g/2 \rfloor$-dimensional component of Y^{-}_{2g}.

As mentioned in the introduction, some transcendental L-functions representing the symplectic case with $(d, N) = (4, 1)$ are already in the LMFDB. The $d = 4$ cases with somewhat larger conductors should be within computational reach.

Acknowledgments

The authors thank Ralf Schmidt and Akshay Venkatesh for helpful conversations.

References

[1] Avner Ash and David Pollack, *Everywhere unramified automorphic cohomology for* $\mathrm{SL}_3(\mathbb{Z})$, Int. J. Number Theory **4** (2008), no. 4, 663–675, DOI 10.1142/S1793042108001602. MR2441799

[2] Jonathan Bober, J. Brian Conrey, David W. Farmer, Akio Fujii, Sally Koutsoliotas, Stefan Lemurell, Michael Rubinstein, and Hiroyuki Yoshida, *The highest lowest zero of general L-functions*, J. Number Theory **147** (2015), 364–373, DOI 10.1016/j.jnt.2014.07.023. MR3276330

[3] Ce Bian, *Computing* GL(3) *automorphic forms*, Bull. Lond. Math. Soc. **42** (2010), no. 5, 827–842, DOI 10.1112/blms/bdq038. MR2721743

[4] Andrew R. Booker, *Uncovering a new L-function*, Notices Amer. Math. Soc. **55** (2008), no. 9, 1088–1094. MR2451344

[5] Luis Dieulefait and Núria Vila, *Geometric families of 4-dimensional Galois representations with generically large images*, Math. Z. **259** (2008), no. 4, 879–893, DOI 10.1007/s00209-007-0253-x. MR2403746

[6] David W. Farmer, Sally Koutsoliotas, and Stefan Lemurell, *Maass forms on* GL(3) *and* GL(4), Int. Math. Res. Not. IMRN **22** (2014), 6276–6301, DOI 10.1093/imrn/rnt145. MR3283005

[7] David W. Farmer, Sally Koutsoliotas, and Stefan Lemurell, *Varieties via their L-functions*, J. Number Theory **196** (2019), 364–380, DOI 10.1016/j.jnt.2018.01.019. MR3906483

[8] `https://github.com/davidfarmer/LandscapeData`

[9] David W. Farmer, Ameya Pitale, Nathan C. Ryan, and Ralf Schmidt, *Analytic L-functions: definitions, theorems, and connections*, Bull. Amer. Math. Soc. (N.S.) **56** (2019), no. 2, 261–280, DOI 10.1090/bull/1646. MR3923345

[10] Dorian Goldfeld, *Automorphic forms and L-functions for the group* $\mathrm{GL}(n, \mathbf{R})$, Cambridge Studies in Advanced Mathematics, vol. 99, Cambridge University Press, Cambridge, 2006. With an appendix by Kevin A. Broughan, DOI 10.1017/CBO9780511542923. MR2254662

[11] Sigurdur Helgason, *Groups and geometric analysis*, Pure and Applied Mathematics, vol. 113, Academic Press, Inc., Orlando, FL, 1984. Integral geometry, invariant differential operators, and spherical functions. MR754767

[12] John W. Jones and David P. Roberts, *Timing analysis of targeted Hunter searches*, Algorithmic number theory (Portland, OR, 1998), Lecture Notes in Comput. Sci., vol. 1423, Springer, Berlin, 1998, pp. 412–423, DOI 10.1007/BFb0054880. MR1726089

[13] John W. Jones and David P. Roberts, *Artin L-functions of small conductor*, Res. Number Theory **3** (2017), Paper No. 16, 33, DOI 10.1007/s40993-017-0079-5. MR3669395

[14] Elon Lindenstrauss and Akshay Venkatesh, *Existence and Weyl's law for spherical cusp forms*, Geom. Funct. Anal. **17** (2007), no. 1, 220–251, DOI 10.1007/s00039-006-0589-0. MR2306657

[15] `https://github.com/lemurell/Euler/`

[16] The LMFDB Collaboration, The L-functions and modular forms database, `https://www.lmfdb.org`, 2023.

[17] I. G. Macdonald, *Spherical functions on a* $\mathfrak{p}$*-adic Chevalley group*, Bull. Amer. Math. Soc. **74** (1968), 520–525, DOI 10.1090/S0002-9904-1968-11989-5. MR222089

[18] Jean-François Mestre, *Formules explicites et minorations de conducteurs de variétés algébriques* (French), Compositio Math. **58** (1986), no. 2, 209–232. MR844410

[19] Stephen D. Miller, *The highest lowest zero and other applications of positivity*, Duke Math. J. **112** (2002), no. 1, 83–116, DOI 10.1215/S0012-9074-02-11213-7. MR1890648

[20] Stephen D. Miller, *On the existence and temperedness of cusp forms for* $\mathrm{SL}_3(\mathbb{Z})$, J. Reine Angew. Math. **533** (2001), 127–169, DOI 10.1515/crll.2001.029. MR1823867

[21] A. M. Odlyzko, *Lower bounds for discriminants of number fields*, Acta Arith. **29** (1976), no. 3, 275–297, DOI 10.4064/aa-29-3-275-297. MR401704

[22] Jasper Scholten, *A non-selfdual 4-dimensional Galois representation*, Preprint, `arXiv:math/9905219`.

[23] Gunther Steil, *Eigenvalues of the Laplacian and of the Hecke operators for* $PSL(2, Z)$, Report number: DESY-94-028, online `https://inspirehep.net/literature/372116`.

[24] Andreas Strömbergsson, *On the zeros of L-functions associated to Maass waveforms*, Internat. Math. Res. Notices 1999, no. 15, 839–851.

[25] Bert van Geemen, Wilberd van der Kallen, Jaap Top, and Alain Verberkmoes, *Hecke eigenforms in the cohomology of congruence subgroups of* $\mathrm{SL}(3, \mathbf{Z})$, Experiment. Math. **6** (1997), no. 2, 163–174. MR1474576

[26] Bert van Geemen and Jaap Top, *A non-selfdual automorphic representation of* GL_3 *and a Galois representation*, Invent. Math. **117** (1994), no. 3, 391–401, DOI 10.1007/BF01232250. MR1283724

American Institute of Mathematics
Email address: `farmer@aimath.org`

Bucknell University
Email address: `s.koutsoliotas@bucknell.edu`

Chalmers University of Technology and University of Gothenburg
Email address: `sj@chalmers.se`

University of Minnesota Morris
Email address: `roberts@morris.umn.edu`